ELSEVIER

Journal of Power Sources 85 (2000) 172–177

JOURNAL OF POWER SOURCES

www.elsevier.com/locate/jpowsour

Development of VRLA batteries for high rate discharge applications

Jenn-Shing Chen

Department of Chemical Engineering, I-Shou University, Kaohsiung County 840, Taiwan

Accepted 22 September 1999

Abstract

During high-rate discharge, there is less utilization of the sealed, valve-regulated lead/acid VRSLA batteries because the secondary current distribution is less uniform and there is less time for ion diffusion. This study investigated the effects of positive plates' material porosity, positive/negative active material ratio, and electrode stacking pressure on cell performance during high-rate discharge. According to the experimental results, the cells with a porosity of 74–76% and positive/negative active material ratio of 1.2–1.5 exhibited the best cell performance. Cells with higher electrode stacking pressure exhibited higher initial capacity and average capacity per cycle with lower capacity loss per cycle.

Keywords: Valve-regulated lead/acid cell; High-rate discharge; Positive plates; Electrode stacking pressure; Porosity

1. Introduction

The sealed valve-regulated lead/acid battery (VRLA) was developed in the first half of the 1960s for use in portable equipment. Subsequently, the technology was successfully introduced into larger units, and today sealed batteries are used in a number of applications challenging their conventional counterparts in almost all applications [1,2]. In recent years, sealed batteries have been developed to suit specific applications with characteristics that make them more appropriate for these particular applications. When used for uninterruptible power supplies (UPS), a short operation time is more useful because of shortened power failure time due to enhanced commercial power supply reliability. The main requirements for UPS batteries are long life, individual battery performance equalization within a battery pack, low cost, and high-rate discharge performance. The high-rate discharge requirements normally enable a 10-min back up during 3 C discharge [3]. In this paper, the design of sealed lead-acid batteries for high-rate discharge was studied.

Generally, at higher discharge rates, ohmic charge-transfer, and mass-transfer effects become significant in polarizing the battery system [4]. At high-rate discharge, there is less utilization in VRLA batteries because the secondary current distribution is less uniform and there is less time for electrolyte ion diffusion. There are several methods to increase high-rate positive plate performance through design:

(i) grid alloy geometry variation, or the addition of conducting materials to the electrode active materials to increase uniform secondary current distribution;
(ii) using thinner plates or larger plate material porosity to increase the total surface area [5];
(iii) increasing the positive/negative active material ratio to increase the positive material capacity;
(iv) increasing the electrode stacking pressure or electrolyte concentration to improve the mass transfer effect;
(v) improvement of the relevant features such as grid-frame, take-off lugs, top lead, separator arrangement, terminal materials and intercell-connector to reduce ohmic effects.

Although higher capacity at high-rate discharge can be obtained by increasing the total surface area or positive material capacity, the battery cycle life will be reduced. In this work, we examined the effects of positive plate mate-

0378-7753/00/$ - see front matter
PII: S0378-7753(99)00397-3

rial porosity, electrode stacking pressure, and the positive/negative active material ratio on the VRLA battery capacity and cycle life at high-rate discharge.

2. Experimental procedures

2.1. Cell construction

Three groups of cells were tested. Table 1 provides a summary of the different groups of 2 V VRLA cells with absorptive glass mat (AGM) construction which were tested. Each cell contained two positive plates and three negative plates. Positive paste was prepared by mixing leady oxide with water, sulfuric acid and fiber. The paste compositions were 50 kg ball-mill leady oxide, 6000 cm^3 water, 3500 cm^3 sulfuric acid of 1.40 specific gravity and 50 g short fiber. Mixing was continued for 35 min and the paste's apparent density was 4.1 g cm^{-3}. Next, the paste was applied to grids cast from a Pb/Ca alloy. The grid sizes were 65×39 mm. The positive plates were controlled with around 33 g paste on both sides of each grid and, then, were cured. Curing was performed for one day at temperatures of 45°C at a relative humidity $> 90\%$. Prior to electroformation, the plates were dried in air about 3–5 days until the moisture in the paste < 1 wt.%. The current density was controlled at 6 mA/cm^2 and the formation capacity had a theoretical capacity of about 200% in the formation conditions. After formation, the plates were washed in running water for several hours and then dried in an oven at 65°C for 24 h. All negative plates and AGM separators used in this work were furnished by Cheng Kwang Battery (Taiwan). Each cell was filled with 38 cm^3 of electrolyte and then sealed with a cover. In all experiments, the electrolyte was a sulfuric acid solution having a specific gravity of 1.335 (20°C). The cell's rated capacity is 4 A h.

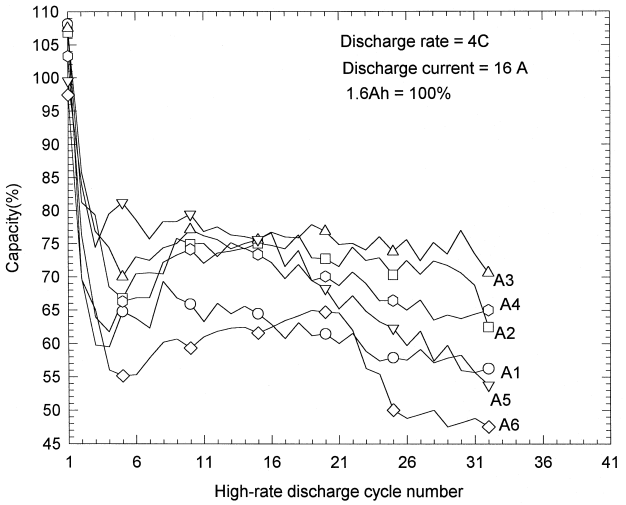

Fig. 1. Capacity vs. high-rate discharge cycle number for the A-cell group.

2.2. Cell cycling tests

Cells were cycled under computer controlled charge and discharge regimens using the Arbin Battery Testing System. To render the cell active, all cells were charged at 0.23 A for 13 h before high-rate cycle testing. The high-rate discharge cycling test consisted of five standard cycles followed by a 4 C high-rate discharge procedure, which consisted of a 16 A discharge to a 1.3 V cutoff and a 0.4 A charge current to the 130% previous discharge capacity. The standard cycle testing employed a discharge current of 0.8 A to 1.75 V cell cutoff voltage and a charge current of 0.4 A to the 120% previous discharge capacity. In addition an open circuit period of 30 min was implemented at the end of each half-cycle. Capacity was measured after every cycle at high-rate discharge. The high-rate discharge cycling test continued for 30–32 cycles.

Table 1
Summary of A, B, C group cell design

Group	Cell	Weight of positive plate (g)	Positive plate thickness (mm)	Porosity (%)	Ratio of active mass [2(+)/3(−)]	Thickness of cell case (mm)	Negative plate weight (g) and thickness (mm)
A	A1	42	3.5	78			27 g and 2.1 mm
	A2	43	3.4	76			27 g and 2.1 mm
	A3	43	3.3	75	1.29		27 g and 2.1 mm
	A4	45	3.5	74	1.29	21	27 g and 2.1 mm
	A5	43	3.1	73	1.43		27 g and 2.1 mm
	A6	45	3.2	71			27 g and 2.1 mm
B	B1	43	3.3	75	1.18		28 g and 2.0 mm
	B2	43	3.3	75	1.29		27 g and 2.0 mm
	B3	43	3.3	75	1.44	21	26 g and 2.0 mm
	B4	43	3.3	75	1.62		25 g and 2.0 mm
	B5	43	3.3	75	1.85		24 g and 2.0 mm
C	C1	41	3.1	76		21	26 g and 2.0 mm
	C2	41	3.1	76		20	26 g and 2.0 mm
	C3	41	3.1	76		19	26 g and 2.0 mm
	C4	41	3.1	76		18	26 g and 2.0 mm

2.3. Analysis of positive plate material

The positive material's physicochemical properties, including the phase composition, and morphology, were obtained using X-ray powder diffraction (XRD), and Scanning electron microscope (SEM) method. All analytic samples taken from the plates were treated by the following steps: [6]

(i) Wash with distilled water (to remove acid);
(ii) Wash with absolute ethanol (to removed water) and drying in desiccator;
(iii) After drying, a portion of each sample was gently ground using a pestle and mortar.

3. Results and discussion

This work attempts/aims to determine the effects of positive plate material porosity, positive/negative active material ratio and electrode stacking pressure on the cells' performance at high-rate discharge. Three groups (A, B, and C) were studied to assess the influence of porosity, positive/negative active material ratio, and electrode stacking pressure. The summary of the A, B, and C group cell design are listed in Table 1. In order to increase the reliability of the experimental results, a total of 5 cells in each group type was fabricated and subjected to high-rate discharge cycling tests. Fig. 1 shows a plot of high-rate discharge capacity versus high-rate discharge cycle number for the A-cell group. In the figure, cells with greater porosity exhibited a higher initial capacity. However, cell A1 with the largest porosity (78%) showed a lower capacity after several cycles. Table 2 lists the capacity loss rate values and the average delivered capacity per cycle. Both are based on the cell performance at high-rate discharge capacity. The capacity loss rate, expressed as %/cycle, is based on the initial cell high-rate capacity and can be estimated using [7]

$$Y = \left(1 - C_{+}^{1/n}\right) \times 100$$

where n denotes the total cycle number, C_{+} represents the terminal fractional capacity (based on the initial cell capacity), and Y is the average fractional capacity loss for each cycle. According to Table 2, cell A1 in the A-cell group has a higher initial capacity but a higher capacity loss per cycle. The results of A-cell group testing showed that increasing the porosity value resulted in a higher of active material utilization and high-rate discharge capacity. However, plates with too great a porosity have poorer mechanical strength which causes a higher capacity loss for each

Table 2
High-rate discharge performance data for representative groups of 4.0 A h VRLA cells

Sample	Cycle number	Initial capacity (A h)	Capacity loss/cycle (%)	Average capacity/cycle (A h)
Group A				
A1	32	1.73	0.0202	1.011
A2	32	1.71	0.0166	1.180
A3	32	1.72	0.0130	1.220
A4	32	1.65	0.0144	1.120
A5	32	1.59	0.0191	1.140
A6	32	1.56	0.0222	0.947
Group B				
B1	32	1.66	0.0128	1.250
B2	32	1.72	0.0130	1.220
B3	32	1.73	0.0157	1.214
B4	32	1.73	0.0167	1.146
B5	32	1.71	0.0213	1.078
Group C				
C1	31	1.42	0.0138	1.014
C2	31	1.60	0.0149	1.094
C3	31	1.64	0.0132	1.171
C4	31	1.62	0.0137	1.158

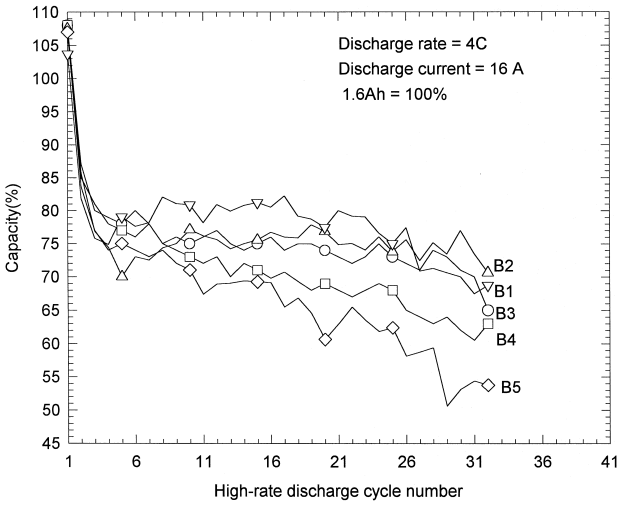

Fig. 2. Capacity vs. high-rate discharge cycle number for the B-cell group.

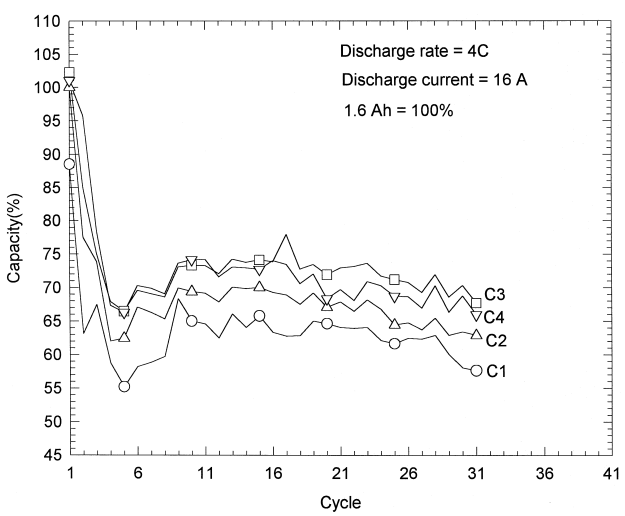

Fig. 3. Capacity vs. high-rate discharge cycle number for the C-cell group.

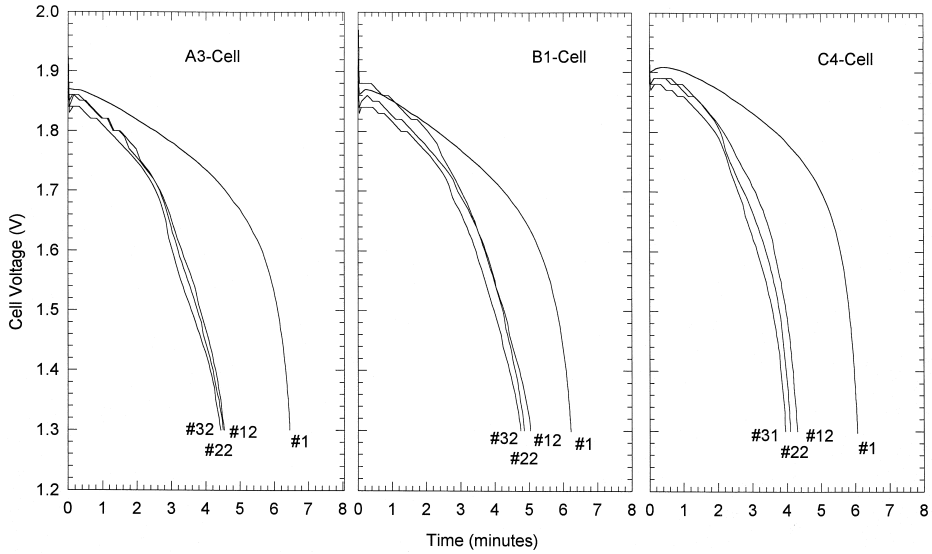

Fig. 4. Cell voltage at various high-rate discharge cycles for cells A3, B1 and C4.

cycle. The cells with porosity of 74–76% exhibited the best high-rate discharge performance in the A-cell group. Fig. 2 shows a plot of the high-rate discharge capacity versus high-rate discharge cycle number for the B-cell group. All of cells in the B-cell group contained the same positive electrode active mass but different amounts of negative electrode active mass. Since the VRLA cell capacity is determined by the positive electrodes, all of the cells in the B-cell group showed a similar capacity in the initial cycles. From Table 2, increasing the positive/negative active material ratio gave rise to a higher capacity loss for each cycle and a shorter cycle life. Cell B5 exhibited a higher initial capacity but a shorter cycle life. The shorter cycle life of cell B5 can be attributed to lower gas-recombination efficiency when the cell was charging. The gas-recombination efficiency relies heavily on the positive/negative active material ratio. Increasing the positive/negative active material ratio causes lower gas-recombination

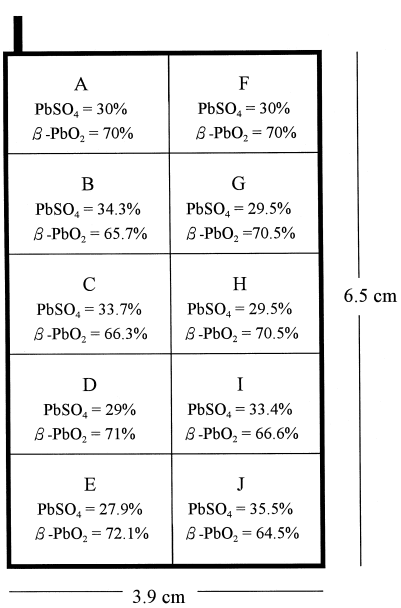

Fig. 5. The X-ray power diffraction phase composition analysis of positive electrodes at A–J, 10 different areas in cell B4 after 32 high-rate discharges.

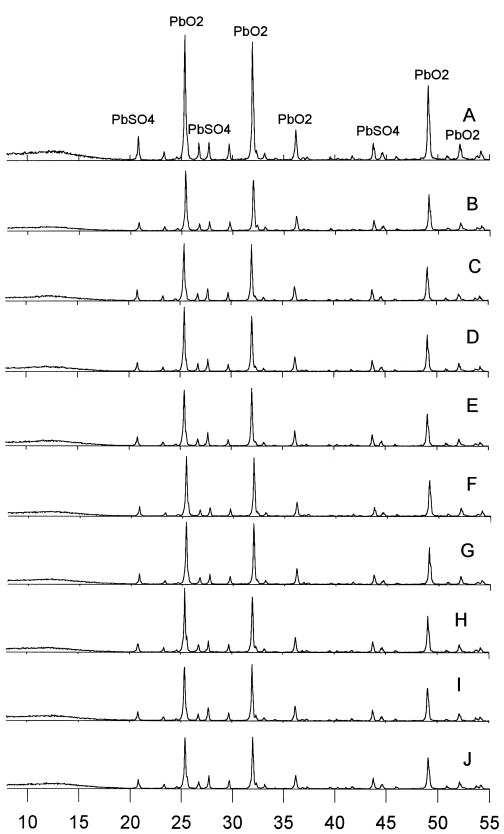

Fig. 6. The X-ray power diffraction patterns for A–J samples expressed in Fig. 5.

efficiency and shorter cycle life or higher capacity loss for each cycle. The best cell performance showed that the best positive/negative active material ratio was about 1.2–1.5. Fig. 3 shows a plot for high-rate discharge capacity versus high-rate discharge cycle number for the C-cell group. Cells C3 and C4, with larger electrode stacking pressure, exhibited higher initial capacity and average capacity per cycle with lower capacity loss per cycle. The higher electrode stacking pressure, having a better mass transfer effect, resulted in the higher capacity. Although, the higher electrode stacking pressure showed the better cell performance at high-rate discharge, cell assembly will be more difficult if electrode stacking pressure is increased. Fig. 4 depicts the cell voltage at various high-rate discharge cycles for cells A3, B1, and C4. As the data reveals, all cells exhibited the expected shapes for high-rate discharge curves. At high-rate discharge, the initial cell voltage dropped considerably. As the cycle number increased, the internal resistance increased causing larger initial cell voltage drops. Also, the cell voltage declined more rapidly, leading to a shorter service life.

The phase composition of the electrodes at different locations was determined after the cells completed high-rate cycle testing. Fig. 5 showed the XRD analyses of phase composition of positive electrodes at 10 different locations in the B4 cell after 32 high-rate discharges. Fig. 6 shows the XRD patterns for the A–J samples expressed in Fig. 5. The results show that the major plate constituent is β-PbO_2 together with some $PbSO_4$. The active material utilization is very low in all of areas. However, the areas of A, B, C, I and J contained large amounts of $PbSO_4$ and revealed a relative higher utilization. The higher utilization of electrode plates at high-rate discharge occurred through the terminal and diagonal areas. The two distinct areas of the various positive electrode samples harvested from two B4 cells were examined microscopically using a SEM. This examination permits an assessment of the physical and chemical variations over microscopic areas of the electrodes. Fig. 7 presents scanning electron micrographs of A and E areas in the positive electrodes after 32 high-rate discharges and a PbO_2 sample. The positive active material exhibited typical development of crystalline PbO_2 (Fig. 7a) and each grain consists of many subgrains. The discharged positive plates in A and E areas (Fig. 7b and c) consist of PbO_2 crystals together with some block-like crystals of $PbSO_4$. Similar to the results with the XRD analyses of phase composition, the major plate constituent is β-PbO_2 together with some $PbSO_4$. Fig. 8 shows the scanning electron micrographs of A and E areas in the positive electrodes after charged from the B4 cell which

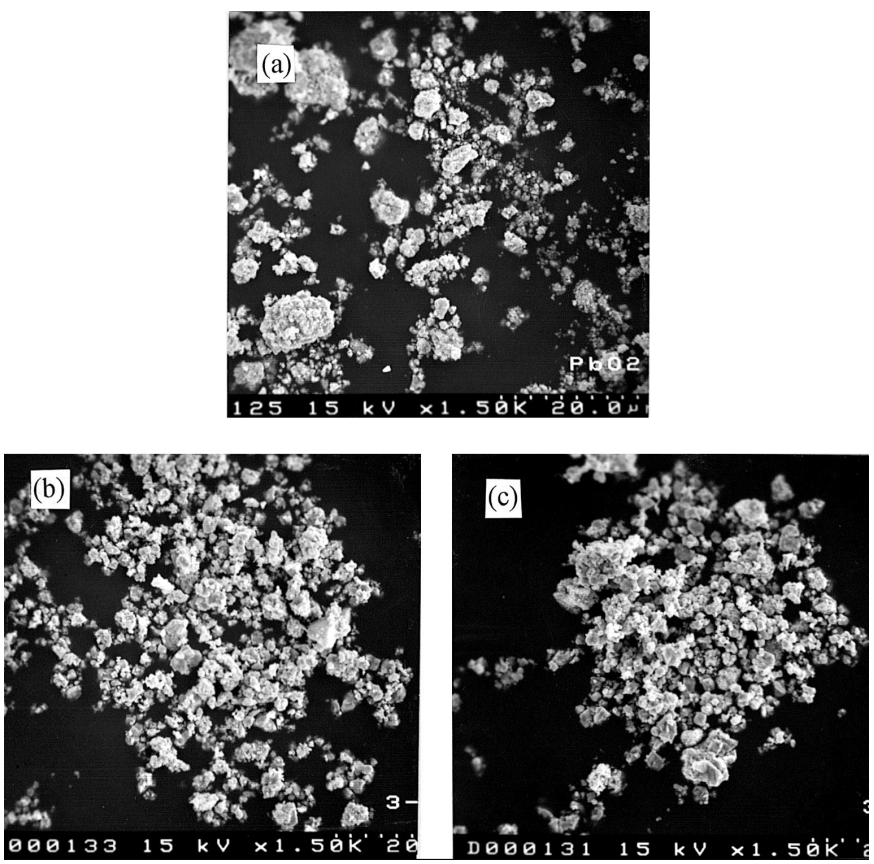

Fig. 7. Scanning electron micrographs of A and E areas in the positive electrodes after 32 high-rated discharges and a PbO_2 sample: (a) PbO_2 sample; (b) A area; (c) E area.

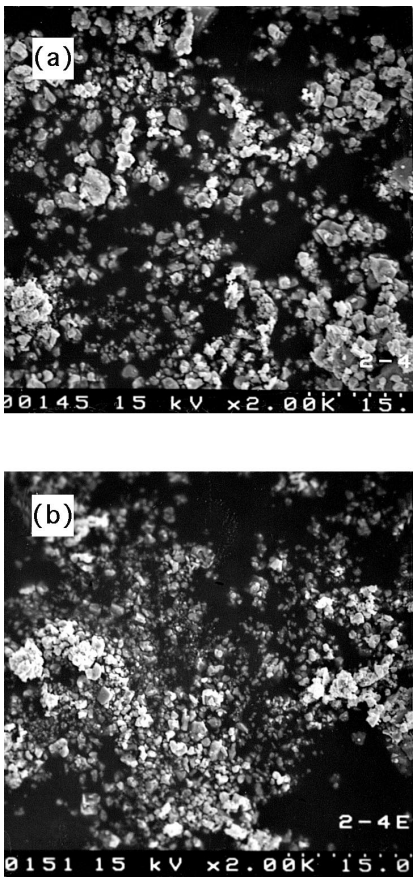

Fig. 8. Scanning electron micrographs of A and E areas in the positive electrodes after charged from the B4 cell which has been through 32 high-rated discharges: (a) A area; (b) E area.

has been through 32 high-rated discharges. The charged plates consist of β-PbO_2 crystals together with a small amount of $PbSO_4$ crystals. This result indicates that some of the active materials have been converted to an inactive form and caused the cell capacity loss.

4. Conclusions

This work attempted to determine the effects of positive plate material porosity, positive/negative active material ratio and electrode stacking pressure on cell performance at high-rate discharge. Based on the results presented above, the following conclusions can be made.

(1) Large positive plate material porosity with a greater total surface area resulted in a higher utilization of active materials and high-rate discharge capacity. However, too great a porosity caused poorer mechanical strength and higher capacity loss for each cycle. The cells with porosity of 74–76% exhibited the best performance.

(2) Increasing the positive/negative active material ratio gave rise to a higher capacity loss for each cycle and a shorter cycle life. The shorter cycle life can be attributed to lower gas-recombination efficiency when the cells were charged. A positive/negative active material ratio of 1.2–1.5 showed the best performance.

(3) Cells with greater electrode stacking pressure exhibited higher initial capacity and average capacity per cycle with lower capacity loss per cycle. Although, the higher electrode stacking pressure showed the better cell performance at high-rate discharge, cell assembly will be more difficult if the electrode stacking pressure is increased.

(4) XRD analyses of phase composition show that the major plate constituent is β-PbO_2 together with some $PbSO_4$ after the cell was high-rate discharged. The active material utilization is very low in all of areas. However, the areas of A, B, C, I and J contained large amounts of $PbSO_4$ and revealed a relative higher utilization. The higher utilization of electrode plates at high-rate discharge occurred through the terminal and diagonal areas.

Acknowledgements

This author would like to thank the National Science Council of the R.O.C. for financially supporting this work under Contract No. NSC-87-2214-E-214-001. Thanks are also due to Cheng Kwang Battery, Taiwan for providing several electrodes and cell parts.

References

[1] D.A.J. Rand, J. Power Sources 64 (1997) 157–174.
[2] H. Tuphorn, J. Power Sources 31 (1990) 57–67.
[3] J. Yamashita, H. Nakashima, Y. Kasai, J. Power Sources 36 (1991) 479–495.
[4] J.-S. Chen, H.Y. Cheh, J. Electrochem. Soc. 140 (1993) 1205–1212.
[5] P.T. Moseley, J. Power Sources 64 (1997) 47–50.
[6] J.-S. Chen, L.F. Wang, J. Power Sources 70 (1998) 269–275.
[7] J.-S. Chen, L.F. Wang, J. Appl. Electrochem. 26 (1996) 227–230.